Ocean Engineering ▮ (▮▮▮▮) ▮▮▮–▮▮▮

Contents lists available at ScienceDirect

Ocean Engineering

journal homepage: www.elsevier.com/locate/oceaneng

Investigation of a method for predicting AUV derivatives

E.A. de Barros [a,*], A. Pascoal [b], E. de Sa [c]

[a] Department of Mechatronics Engineering and Mechanical Systems, University of São Paulo. Av. Prof. Mello Moraes, 2231, 05508-900 SP, Brazil
[b] Institute for Systems and Robotics (ISR) and Department of Electrical Engineering and Computers, Instituto Superior Técnico, Av. Rovisco Pais, 1049-001 Lisbon, Portugal
[c] National Institute of Oceanography, Dona Paula, Goa 403 004, India

ARTICLE INFO

Article history:
Received 31 January 2007
Accepted 3 August 2008

Keywords:
AUV
Hydrodynamic derivatives
Prediction method
Manoeuvring
CFD
Slender body

ABSTRACT

The paper addresses the problem of autonomous underwater vehicle (AUV) modelling and parameter estimation as a means to predict the dynamic performance of underwater vehicles and thus provide solid guidelines during their design phase. The use of analytical and semi-empirical (ASE) methods to estimate the hydrodynamic derivatives of a popular class of AUVs is discussed. A comparison is done with the results obtained by using computational fluid dynamics to evaluate the bare hull lift force distribution around a fully submerged body. An application is made to the estimation of the hydrodynamic derivatives of the MAYA AUV, an autonomous underwater vehicle developed under a joint Indian-Portuguese project. The estimates obtained were used to predict the turning diameter of the vehicle during sea trials.

1. Introduction

Predicting the manoeuvring performance of an autonomous underwater vehicle (AUV) is important during the vehicle's design phase. Techniques for estimating the hydrodynamic coefficients of fully submerged vehicles can be traced back to the tools originally developed to predict the aerodynamic coefficients of airships, later refined for aircraft and missiles, and subsequently adopted for submarines. Methods for estimating hydrodynamic derivatives have also been used in the ship industry for decades.

Recently, spawned by the widespread availability of powerful computers, there has been a surge of interest in applying computational fluid dynamics (CFD) for constructing the flow field and calculating the pressure distribution acting upon a submerged marine vehicle. From such maps, the resulting forces and moments of interest acting on the vehicle can be calculated.

Tank tests using a constrained vehicle model can also be used to estimate its hydrodynamic coefficients. Another experimental approach relies on tests with free running models in basins or in natural areas (lakes, open sea, etc.). Both approaches are time consuming and expensive. They involve model building, testing, analyzing and interpreting the results. Costs can be even higher if the option to rely on an experimental approach is taken at the preliminary design phase. In fact, the vehicle configuration may be changed many times for non-hydrodynamic-related reasons, thus reducing considerably the usefulness of early test results.

Analytical and semi-empirical (ASE) methods for the estimation of vehicle hydrodynamic derivatives yield approximate results that can be used to predict manoeuvrability characteristics, select hydroplanes, and investigate control strategies at an early stage in a new design. The application of ASE methods to parameter estimation for submarines and AUVs has been described in the literature. See for example Humphreys (1981), Maeda and Tatsuta (1989), Nahon (1993, 1996), Bohlmann (1990), Prestero (2001), and Ridley et al. (2003) and the references therein. Advanced approaches to AUV design may also involve combined plant/controller optimization (Silvestre et al., 1998), where the prediction of hydrodynamic derivatives based on the vehicle's geometrical description plays a key role.

To the best of our knowledge, no in-depth systematic study has been done to evaluate and validate the above methods for the identification of AUV dynamics. It is important to try and compare the types of estimates that are obtained with ASE and CFD methods and judge the accuracy of these estimates by resorting to towing tank and model basin experiments. This type of information will certainly play a major role during the vehicle design phase so as to meet open-loop requirements. At the same time, once bounds are known for inaccuracies that are inherent in prediction methods, better control approaches can be devised to explicitly deal in closed loop with the uncertainties associated with the design models obtained.

This work is a contribution towards meeting the above-mentioned goals. The paper guides the reader through estimation of the hydrodynamic derivatives of slender-type AUVs using information available from a number of sources, mainly the aircraft Datcom (Hoak and Finck, 1978) handbook and missile-related literature (Pitts et al., 1957; Nielsen, 1960; Jorgensen, 1977).

* Corresponding author. Tel.: +55 11 3091 5761; fax: +55 3091 5471.
E-mail address: eabarros@usp.br (E.A. de Barros).

0029-8018/$ - see front matter © 2008 Elsevier Ltd. All rights reserved.
doi:10.1016/j.oceaneng.2008.08.008

An application is made to the estimation of a set of derivatives for the MAYA AUV, an autonomous vehicle developed under a joint Indian-Portuguese project. The paper is organized as follows. Section 2 introduces the main concepts and formulas that have been investigated for estimating the hull lift and drag-related derivatives. A comparative analysis between ASE and CFD results is presented. Section 3 presents the lift and drag coefficients for small aspect lift surfaces and describes the formulation adopted in this paper for the combined fin and hull derivatives. Section 4 discusses the impact of propeller ducts on the estimates of the derivatives. Section 5 exploits the results obtained in the previous sections to compute the stability derivatives for the lateral and dive planes and presents a comparison of the actual turning manoeuvre diameter of the vehicle against its predicted value. Section 6 contains the main conclusions of the work done so far along with future formulations and steps for validating ASE methods.

2. Bare hull coefficients

Axisymmetric geometry is a common shape for AUVs and also for torpedoes and missiles. Among them, the shape proposed by Myring (1976) has been chosen extensively for calculations and experimental validation. This shape was adopted in AUVs such as the REMUS (Prestero, 2001) and the MAYA (de Barros et al., 2004). The Myring geometry affords the designer practical advantages related to the availability of inner space for carrying equipment while keeping the more streamlined characteristics outside, as compared to torpedo shapes. This geometry is therefore appropriate for a study aimed at the construction of a database that can help at the early stages of AUV design.

In what follows, the vehicle length L and its powers are used to define formulas for the estimation of hydrodynamic derivatives according to the non-dimensional standards of SNAME (SNAME, 1950). The forces and moments considered refer to a body-axis system (Fig. 1) whose origin is at the vehicle's centre of mass. The main particulars of the MAYA hull are described in Table 1.

Only velocity-related parameters are discussed in this paper. Computation of added mass coefficients relies only on ideal fluid flow theory. A number of reliable numerical methods are available for estimating these kinds of parameters. Source distribution and panel methods are the most common numerical techniques. Approximating the hull by an ellipsoid and obtaining the parameters from analytical computations is a simplified approach. This latter option was chosen by the authors to compute the surge added mass. For the other coefficients, the strip method was applied (Newman, 1977).

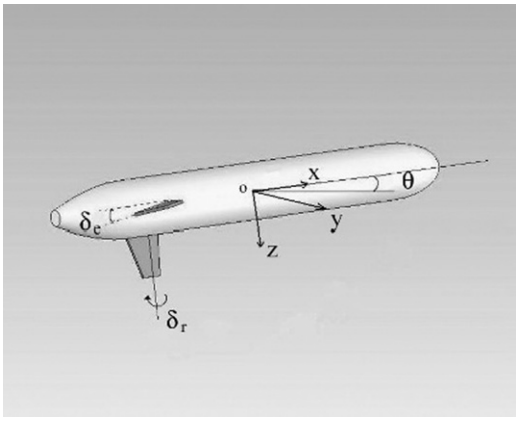

Fig. 1. Representation of the vehicle body-axis system and lift surface angles.

Table 1
Main parameters of the hull

Bare hull length (m)	1.742
Hull maximum diameter (m)	0.234
Base diameter (m)	0.057
Nose length (m)	0.217
Middle body length (m)	1.246
Myring body parameter θ (deg)	25
Myring body parameter n	2

2.1. Lift force and moment

When calculated using SBT for a body of revolution, the lift coefficient of a submerged vehicle, based on the base area, is equal to a value of 2. For a vehicle with a "Myring shape" composed of forebody, cylinder, and afterbody, applying such an approach blindly means that one neglects the vortex and separation produced by viscous effects at the tail region.

In a number of AUVs, the presence of appendages may even intensify the break down of the ideal flow hypothesis before the body base. On the other hand, applying the slender body method only up to the end of the nose section (de Barros et al., 2004), as is routinely done in the case of missiles with a blunt base, means neglecting the pressure distribution at the tail. In this case, applying the Datcom expression to the computation of the lift coefficient yields (Hoak and Finck, 1978)

$$(C_{L_\alpha})_B = \left(\frac{\partial C_{L_\alpha}}{\partial \alpha}\right)_{\alpha=0} = \frac{2(k_2 - k_1)S_N}{L^2}, \tag{1}$$

where S_N is the cross-sectional area at the end of the nose section and "k_2–k_1" is the "Munk" apparent mass factor. For the fineness ratio interval between 4 and 19, this factor can be computed as

$$(k_2 - k_1) = -0.0006548f^2 + 0.0256f + 0.73. \tag{2}$$

The intermediate solution adopted in this paper was to use the Datcom method to estimate the station at an axial distance from body nose, denoted x^*, where the ideal flow hypothesis is no longer valid, and to use the cross-sectional area at such station, denoted S^*, as the reference area for the lift coefficient to obtain

$$(C_{L_\alpha})_B = \frac{2(k_2 - k_1)S^*}{L^2}. \tag{3}$$

The estimate of position x^* is based on the station x_1 where the body profile has the most negative slope in the aft direction. It is intuitive that a phenomenon such as flow separation is likely to occur near this region. The semi-empirical relation between the two distances is given by (Hoak and Finck, 1978)

$$x^* = 0.378L + 0.527x_1. \tag{4}$$

An identical approach can be used to compute the lift moment coefficient of an AUV using the volume V^* between the nose tip and the station at x^*. Manipulating the corresponding Datcom expression gives

$$(C_{m_\alpha})_B = \frac{x_m(C_{L_\alpha})_B}{L} + 2(k_2 - k_1)\frac{V^* - S^*x^*}{L^3}, \tag{5}$$

where x_m is the axial distance from the body nose to pitching-moment reference centre.

At this point, an analysis based on CFD methods can provide an interesting visualization and an important reference for the ASE estimation. Fig. 2 shows the visualization of the pressure distribution of the flow around the body for a range of angles of attack, from 5° to 20°, generated by the program Fluent®, assuming the flow speed as 1.2 m/s. The $K\omega$ turbulence model was adopted.

Please cite this article as: de Barros, E.A., et al., Investigation of a method for predicting AUV derivatives. Ocean Engineering (2008), doi:10.1016/j.oceaneng.2008.08.008

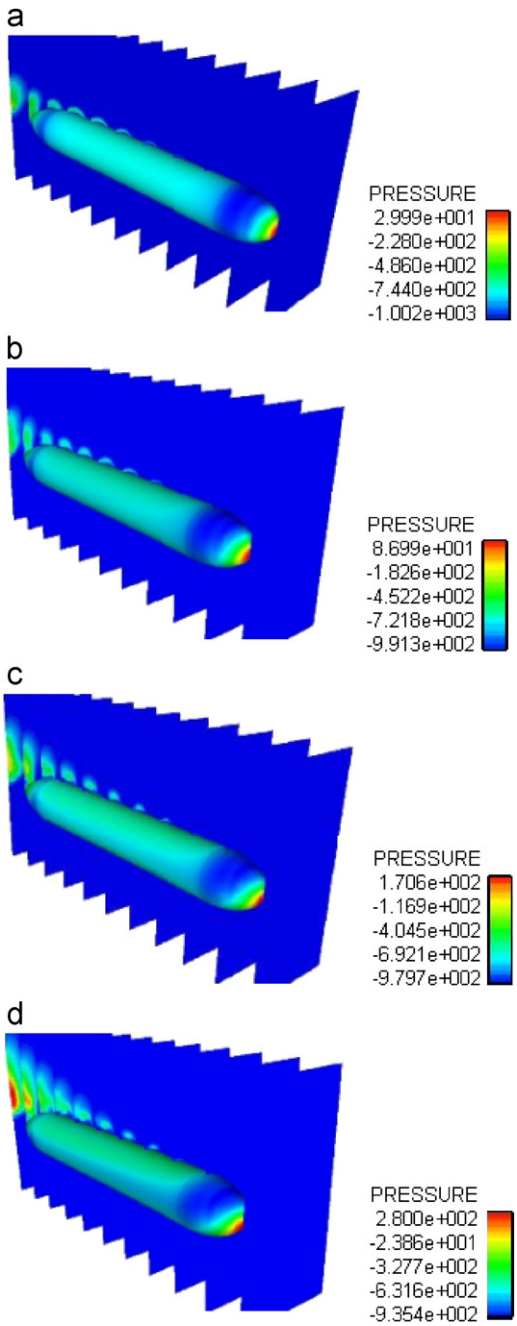

Fig. 2. Pressure distribution around the bare hull.

The relative pressure (total minus dynamic pressure) is represented by different tones around the body. As the angle of attack is increased, increasing pressure from the cylinder to the tail can be observed. Small regions representing the vortices of flow separation from the upper surface of the body can also be seen to increase in number and area as the angle of attack is increased. This is a sign of the growing viscous effect on the flow around the body. As seen in Fig. 2, the large pressure distribution begins to spread around the top of the body and the spreading becomes more accentuated as the angle of attack increases.

Consider now Fig. 3, which shows the pressure variation for a series of angular sections of the body that start at 0° (section containing part of the positive y body-axis) and are rotated counter-clockwise with respect to the z body-axis. Clearly, an increase in pressure occurs also at the bottom of the body, as observed in the pressure variation curve along the 270° section. This curve and the other curve at 90° separate from the others as the angle of attack is increased, and by comparing the amplitude of both it can be verified that the resultant normal force increases upwards.

Fig. 4 shows the normal force coefficient computed by CFD for 5°, 10°, 15° and 20° of angle of attack. The figure shows also the curve generated by the analytical model proposed by Allen Perkins (1951) for the non-linear variation of C_N. According to this model, the normal force coefficient is given by

$$C_N = \frac{S_b}{S_{ref}}\sin(2\alpha)\cos\left(\frac{\alpha}{2}\right) + \eta C_d \frac{S_p}{S_{ref}}\sin^2(\alpha), \tag{6}$$

where S_b is the base area, S_p is the planform area at the xy plane, and S_{ref} is the reference area (taken as L^2 in this work). The coefficient C_d, taken as 1.2, is the steady-state cross flow drag coefficient for an infinitely long circular cylinder. The coefficient η is a correction factor equal to the ratio of C_d for a finite length cylinder to that for an infinite cylinder. This parameter is a function of the fineness ratio.

The moment coefficient C_m is obtained from integration of the normal force coefficient per unit of length along the body as

$$C_m = \frac{1}{L^3}\int_0^L c_N(x)(x_m - x)\,dx. \tag{7}$$

The normal force coefficient per unit of length is given by

$$c_N(x) = \sin(2\alpha)\cos\left(\frac{\alpha}{2}\right)\frac{dS(x)}{dx} + 2\eta C_d \sin^2(\alpha) r(x), \tag{8}$$

where $r(x)$ is the cross section radius at the distance x from the nose tip and $S(x)$ is the corresponding area.

The resulting moment coefficient is

$$C_m = \left[\frac{V - A_b(L - x_m)}{L^2}\right]\sin(2\alpha)\cos\left(\frac{\alpha}{2}\right) + \eta C_{d_\eta}\frac{S_p}{L^2}\left(\frac{x_m - x_c}{L}\right)\sin^2(\alpha), \tag{9}$$

where V is the body volume and x_c is the axial distance from body nose to centroid of body planform area.

Fig. 4 shows very good agreement between the model represented by (6) and the CFD generated results. Good agreement was also shown between the model and results obtained in experiments with blunt base and pointed slender bodies of revolution (Jorgensen, 1977). The first term in (6) represents the contribution from the potential flow, which gives the same result as that obtained using SBT for the coefficient slope at the angle of attack equal to zero. The second term represents the viscous cross flow contribution, which becomes significant as the angle of attack increases.

Fig. 5 represents the lift coefficient slope computed from the model in (1), (3) and the tangent to the curve based on (6), at $\alpha = 0$, which corresponds to the classical result from SBT. It is seen that the intermediate linear model is closer to the model, which represents the real variation of C_N accurately. The figure can also suggest other ways to choose linear approximations, switch among them, and establish bounds for the normal force coefficient.

The CFD result for the lift moment coefficient is also closer to the estimate provided by Datcom in the small angle of attack range. Fig. 6 shows the moment coefficient relative to the centroid of body planform area. Note that this choice for the centre of rotation implies that the viscous term contribution in Eq. (9) is zero. The C_m slope for zero angle of attack according to the Datcom approach (Eq. (5)) was chosen for calculating the moment derivative of MAYA.

The forces and moments caused by the rotational motion of the vehicle are usually more difficult to predict, since viscous effects

Please cite this article as: de Barros, E.A., et al., Investigation of a method for predicting AUV derivatives. Ocean Engineering (2008), doi:10.1016/j.oceaneng.2008.08.008

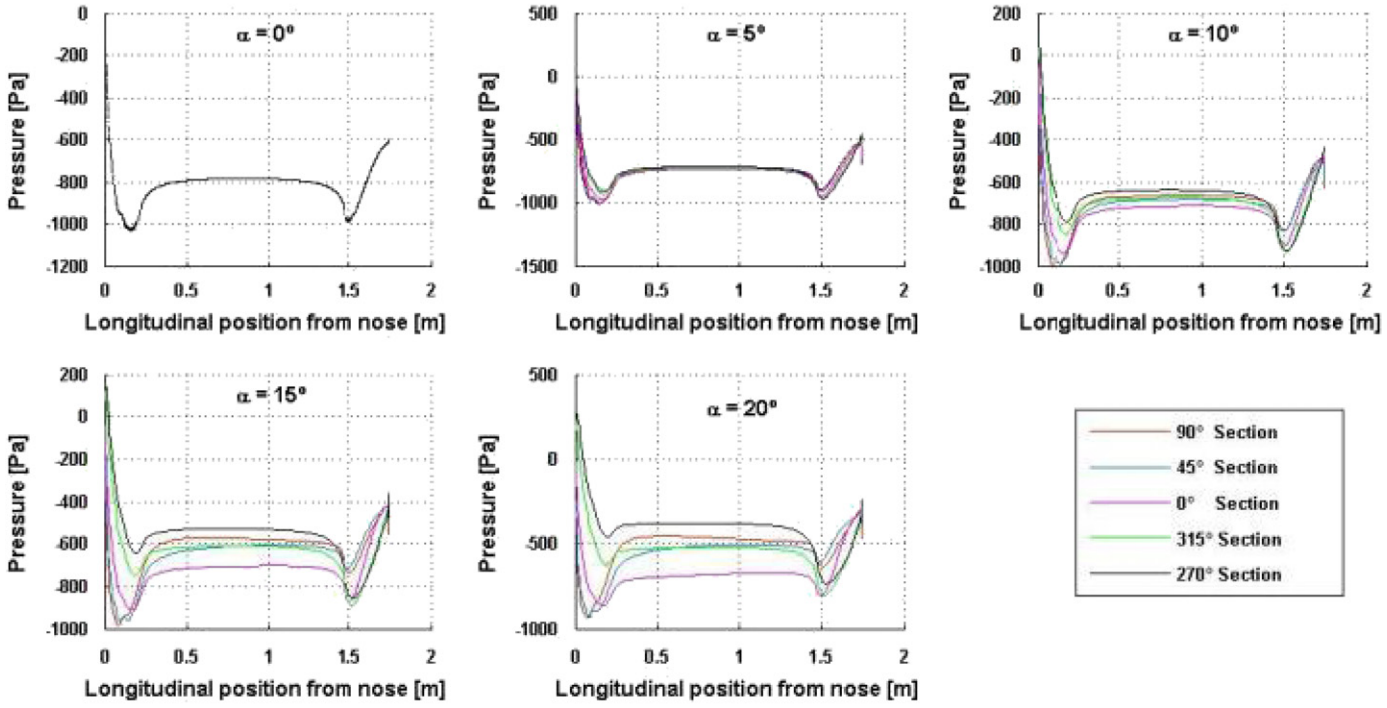

Fig. 3. Pressure distribution along the hull sections.

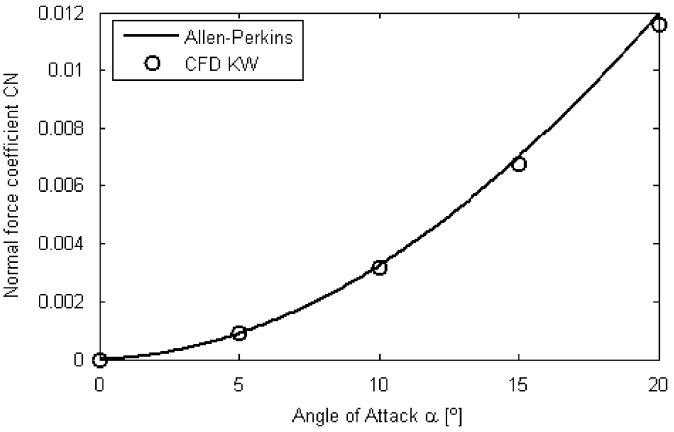

Fig. 4. Comparison between the Allen-Perkins equation and CFD results.

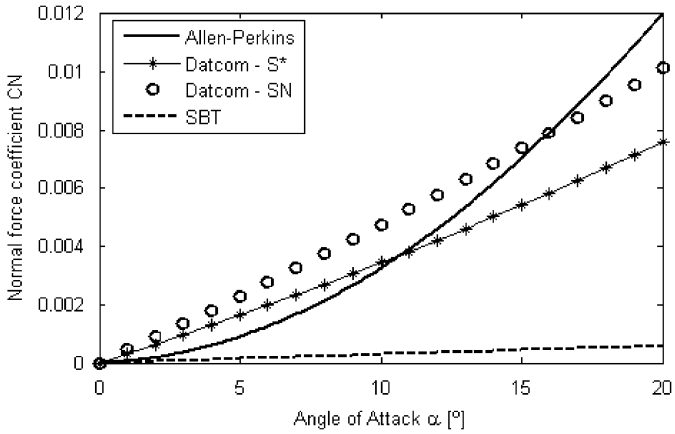

Fig. 5. Comparison of the ASE models: slender body theory (SBT), Datcom using S^*, and S_N as reference areas, respectively.

are significant. The approximation for this class of stability derivatives, adopted in the missile field, is again based on slender body theory. The pitching lift coefficient is given by

$$(C_{L_q})_B = (C_{L_\alpha})_B \left(\frac{L - x_m}{L}\right). \tag{10}$$

The moment damping coefficient is calculated as follows:

$$(C_{m_q})_B = -(C_{L_\alpha})_B \left(\frac{L - x_m}{L}\right)^2 + \frac{(x_b - x_m)}{L^4} V, \tag{11}$$

where x_b is the axial distance from the nose tip to the body centroid.

The second term on the right-hand side of (11) can be often neglected since it is normal practice to take the origin of the system of coordinates at the body centre of gravity whose longitudinal position is as close as possible to that of the centre of buoyancy.

2.2. Hull drag

In the work of Myring (1976), drag was estimated by calculating the axisymmetric boundary layer. Less laborious methods can provide similar results (Chappell, 1978). They are based on knowledge of the fineness ratio of the body (ratio of the body's length to its maximum diameter). The corresponding Datcom formula is based on the latter approach, and was also adopted in this work to yield (see Hoak and Finck, 1978)

$$C_D^* = C_f[1 + 60f^{-3} + 0.0025f]\frac{S_s}{L^2}, \tag{12}$$

Please cite this article as: de Barros, E.A., et al., Investigation of a method for predicting AUV derivatives. Ocean Engineering (2008), doi:10.1016/j.oceaneng.2008.08.008

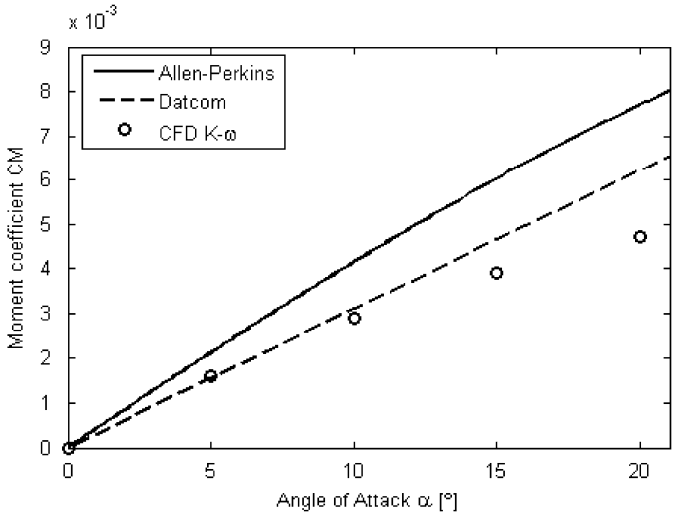

Fig. 6. Moment coefficient variation: CFD and ASE methods.

where S_s is the body wetted area and

$$C_f = \frac{0.075}{(\log Re - 2)^2} + 0.00025 \tag{13}$$

is the estimate of the skin friction drag coefficient, according to ITTC .The parameter f is the fineness ratio of the body, $f = L/d$, relating body length to maximum diameter. The value of C_D^* should be added to the base-drag coefficient

$$C_{D_b} = 0.029\left(\frac{d_b}{d}\right)^3 (C_D^*)^{-0.5}\frac{S_N}{L^2}, \tag{14}$$

where d_b is the base diameter. The complete body drag coefficient is then given by

$$C_{D_0} = C_D^* + C_{D_b}. \tag{15}$$

3. Lift surfaces and body–fin interaction

3.1. Lift and drag produced by small aspect ratio fins

The most extensive study on lift and drag produced by small aspect ratio fins for marine applications was carried out by Whicker and Fehlner (1958), who proposed semi-empirical expressions similar to those adopted for ship and submarine manoeuvring models (Lewis, 1988; Bohlmann, 1990). The lift coefficient of a fin is given by

$$\frac{C_{L_{2W}}}{AR} = \frac{2\pi}{2 + \sqrt{(1/\eta^{*2})((AR^2/\cos^2 \Lambda_{c/4}) + 4\cos^2 \Lambda_{c/4}}}, \tag{16}$$

where AR is the lift surface aspect ratio, $\Lambda_{c/4}$ is the sweep angle at one-fourth of the chord length, and η^* is a factor to correct for viscous effects.

Foil drag contributions are also considered in the present paper. Based on the semi-empirical expression proposed by Hoerner (1985) for streamlined shapes at low Reynolds numbers, the foil drag coefficient is computed as

$$(C_{D_0})_F = \left[2C_f\left(\frac{t}{c}\right)^{-1} + 2C_f + \frac{t}{c}\right]\frac{S_{f(F)}}{L^2}, \tag{17}$$

where t is the foil maximum thickness, c is the corresponding chord, and $S_{f(F)}$ is the maximum cross-sectional area.

3.2. Combined rudder and body coefficients: single fin case

Theoretical and semi-empirical methods have been proposed in the marine and aircraft dynamics fields to estimate the lift produced by a vertical fin in the presence of a body of revolution. See Lewis (1989), Hoak and Finck (1978), and ESDU (1993), respectively, and the references therein. Basically, the methods available capture the body influence at the fin through a change in its aspect ratio. From this parameter, the lift coefficient slope can be calculated using the formula presented in the last section. The horizontal tail can also be accounted for by another influence coefficient obtained from a semi-empirical chart. The approach adopted in this paper is a simplified version of the method proposed in Datcom that does not take into account the influence from the horizontal tail into the flow at the vertical fin.

First, the geometric aspect ratio is calculated for the expanded fin to the hull centre line as (Fig. 7)

$$A_v = \frac{b_v^2}{S_v} \tag{18}$$

The ratio between the effective and the geometric aspect ratio, $f(b_v, r)$, is then determined from the curves in Fig. 8, taking into account the taper ratio value λ_v as function of the span to the hull diameter ratio, $2r$, of the station where the fin is fixed.

The effective aspect ratio is then calculated according to

$$AR_{eff} = f(b_v, r)A_v. \tag{19}$$

The fin side force coefficient, C_{y_β}, is determined from (16), using the effective aspect ratio calculated above. The result is then multiplied by the body-fin empirical interference factor determined in Fig. 9. The final result is

$$C_{y_{\beta(F)}} = -k_v(C_{L_\alpha})_F, \tag{20}$$

$$(C_{y_\beta})_{BF} = (C_{y_\beta})_B + C_{y_{\beta(F)}} - C_{D_{(BF)}}, \tag{21}$$

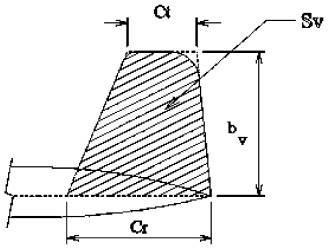

Fig. 7. Parameters and the area considered for calculating the geometric aspect ratio.

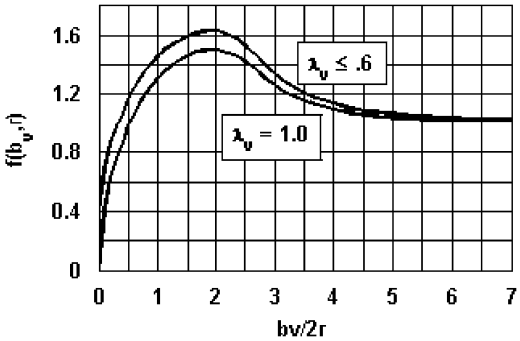

Fig. 8. Ratio of vertical aspect ratio in presence of the bare hull to that of the isolated tail (Hoak and Finck, 1978).

Please cite this article as: de Barros, E.A., et al., Investigation of a method for predicting AUV derivatives. Ocean Engineering (2008), doi:10.1016/j.oceaneng.2008.08.008

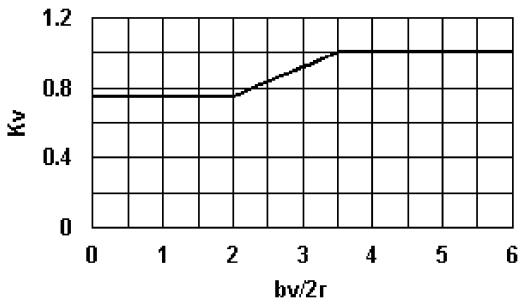

Fig. 9. Empirical factor for estimating the side force due to sideslip of a single vertical tail.

where

$$(C_{y_\beta})_B = -(C_{L_\alpha})_B \tag{22}$$

and

$$C_{D_{(BF)}} = C_{D_0} + C_{D_{0(F)}}. \tag{23}$$

The remaining coefficients for the lateral plane are easily calculated taking into account the distance between the reference centre and the hydrodynamic centre of the vertical fin, as follows:

$$\begin{aligned}(C_{n_\beta})_{(BF)} &= (C_{n_\beta})_B + (C_{y_\beta} - C_{D_0})_{(F)}\frac{(x_O - x_F)}{L}\\ &= -(C_{m_\alpha})_B + (C_{y_\beta} - C_{D_0})_{(F)}\frac{(x_O - x_F)}{L},\end{aligned} \tag{24}$$

$$\begin{aligned}(C_{y_r})_{(BF)} &= (C_{y_r})_B + (C_{y_\beta} - C_{D_0})_{(F)}\frac{(x_O - x_F)}{L}\\ &= -(C_{L_q})_B + (C_{y_\beta} - C_{D_0})_{(F)}\frac{(x_O - x_F)}{L},\end{aligned} \tag{25}$$

$$\begin{aligned}(C_{n_r})_{(BF)} &= (C_{n_r})_B + (C_{y_\beta} + C_{D_0})_{(F)}\frac{(x_O - x_F)^2}{L^2}\\ &= (C_{m_q})_B + (C_{y_\beta} + C_{D_0})_{(F)}\frac{(x_O - x_F)^2}{L^2},\end{aligned} \tag{26}$$

$$(C_{y_{\delta_r}})_{(BF)} = -(C_{y_\beta})_{(F)}, \tag{27}$$

$$(C_{n_{\delta_r}})_{(BF)} = -(C_{y_\beta})_{(F)}\frac{(x_O - x_F)}{L}, \tag{28}$$

where x_O is the axial distance from the body nose to the origin and x_F is the axial distance between the nose tip and the hydrodynamic centre of the fin.

The coefficient C_{y_r} is the side force derivative with respect to yaw rate. The coefficients C_{n_β} and C_{n_r} represent the yaw moment derivative with respect to sideslip angle and yaw rate, respectively. They are calculated using Eqs. (5), (10) and (11), assuming $x_m = x_O$.

Expressions (27) and (28) assume an all movable type of rudder. The roll motion effect is not considered in this study.

3.3. Coefficients for the dive plane

Results derived from SBT (Pitts et al., 1957) can be applied to calculate the lift coefficients produced by the stern plane. In this work, the horizontal bow and stern plane effects were combined with body effects using the classical formulation of lift and lift moment curve slopes. The total lift coefficient, $C_{L_{\alpha(WB)}}$ (where the notation WB borrows from aircraft wing-body interactions) is given by

$$\begin{aligned}C_{L_{\alpha(WB)}} &= C_{L_{\alpha(B)}} + C_{L_{\alpha(W)}} + C_{L_{\alpha B(W)}}\\ &= C_{L_{\alpha(B)}} + (K_{W(B)} + K_{B(W)})(C_{L_\alpha})_e\frac{S_e}{L^2},\end{aligned} \tag{29}$$

where S_e is the total exposed fin surface area, $(C_{L_\alpha})_e$ is the lift coefficient of the exposed fin surfaces, and $K_{B(W)}$ and $K_{W(B)}$ are the interference factors from the surfaces to the body and from the body to the surfaces, respectively. Let b be the maximum span of the fins in combination with the hull, that is, the total distance between the lift surface tips, as if they were extended inside the hull, and define

$$k = \frac{d}{b}. \tag{30}$$

Then, the interference factors can be computed as

$$K_{W(B)} = \frac{2}{\pi}\frac{(1+k^4)\zeta_1 - k^2\zeta_2}{(1-k)^2} \tag{31}$$

and

$$K_{B(W)} = (1+k)^2 - K_{W(B)}, \tag{32}$$

where

$$\zeta_1 = \left[\frac{1}{2}\tan^{-1}\left(\frac{1}{2}(k^{-1} - k)\right) + \frac{\pi}{4}\right] \tag{33}$$

and

$$\zeta_2 = [(k^{-1} - k) + 2\tan^{-1}k]. \tag{34}$$

The estimate of the corresponding moment coefficient $C_{m_{\alpha(WB)}}$ is given by the product of the lift coefficient and the coordinate $x'_{(WB)}$ of the combined hydrodynamic centre normalized by L. To compute $x'_{(WB)}$, start by defining $x'_{W(B)}$ and $x'_{B(W)}$ as the centre of the hull lift carryover on the lift surface and the centre of the fin-lift carryover on the body, respectively. The first is approximated by the hydrodynamic centre position of the fin x'_W (assuming $x_m = x_O$). The latter is given by

$$x'_{B(W)} = \left\{x_O - \left[x_{LE} + \left(\frac{1}{4} + \frac{b-d}{2c_{r_e}}\tan\Lambda_{c/4}P\right)c_{r_e}\right]\right\}\frac{1}{L}. \tag{35}$$

where x_{LE} is the axial distance between the nose tip and the leading edge of the fin at the root chord,

$$\begin{aligned}P = &-\frac{k}{1-k}\\ &+\frac{\sqrt{1-2k}\ln\left(\frac{1-k}{k} + \frac{1}{k}\sqrt{1-2k}\right) - (1-k) + \frac{\pi}{2}k}{\frac{k(1-k)}{\sqrt{1-2k}}\ln\left(\frac{1-k}{k} + \frac{1}{k}\sqrt{1-2k}\right) + \frac{(1-k)^2}{k} - \frac{\pi}{2}(1-k)}\end{aligned} \tag{36}$$

and c_{r_e} is the exposed tip root chord.

This expression assumes that the aspect ratio is greater than or equal to 4. For smaller values of the aspect ratio, $0 \leqslant AR \leqslant 4$, an interpolation procedure should be used, as indicated in Hoak and Finck (1978). The hydrodynamic centre of the combination can be now computed as

$$x'_{(WB)} = \frac{C_{L_{\alpha_{W(B)}}}x'_{W(B)} + C_{L_{\alpha_{B(W)}}}x'_{B(W)} + C_{m_{\alpha_B}}}{C_{L_{\alpha_{(WB)}}}}. \tag{37}$$

Therefore, the static moment coefficient for the combination is given by

$$C_{m_{\alpha_{(WB)}}} = x'_{(WB)}C_{L_{\alpha_{(WB)}}}. \tag{38}$$

To capture the effects due to the deflection of the control surfaces, the elevator coefficients are calculated from the expressions derived in Pitts et al. (1957) as

$$C_{L_{\delta_e}} = (k_{B(W)} + k_{W(B)})(C_{L_\alpha})_e\frac{S_e}{L^2} \tag{39}$$

and

$$C_{m_{\delta_e}} = C_{L_{\delta_e}}x'_W, \tag{40}$$

where δ_e is the deflection angle of the lift surface. The influence factors between hull and lift surface are determined from the

Please cite this article as: de Barros, E.A., et al., Investigation of a method for predicting AUV derivatives. Ocean Engineering (2008), doi:10.1016/j.oceaneng.2008.08.008

relationship

$$k_{B(W)} + k_{W(B)} = K_{W(B)}. \quad (41)$$

The estimation of dynamic coefficients relies on the computation of the lift and moment produced by the fin body combination when the angle of attack is changed at the fin due to the rotational motion. Therefore, taking (29) and (38) into account yields

$$(C_{L_q})_{WB} = (C_{L_q})_B - [K_{W(B)} + K_{B(W)}](C_{L_\alpha})\frac{S_e}{L^2}x'_W \quad (42)$$

and

$$(C_{m_q})_{WB} = (C_{m_q})_B - [K_{W(B)} + K_{B(W)}](C_{L_\alpha})\frac{S_e}{L^2}x'^2_W. \quad (43)$$

4. Duct effect

A number of AUVs are equipped with commercial ducted propellers, usually produced originally for the ROV industry. Ducts can help the AUV accelerate from zero to cruising speed. At cruising speed, however, the duct drag effect may cancel, or even surpass the additional thrust it produces. Moreover, the duct also contributes to increasing damping parameters.

Lift, drag, and moment coefficients have been computed by formulas derived from theoretical results that were validated experimentally for some duct profiles investigated by Morgan and Caster (1965). For the AUV considered in this paper, a duct shape designed for forward thrust increase under cruising motion was considered, see Fig. 10. Fig. 11 shows the theoretical curves for the corresponding lift and moment coefficients.

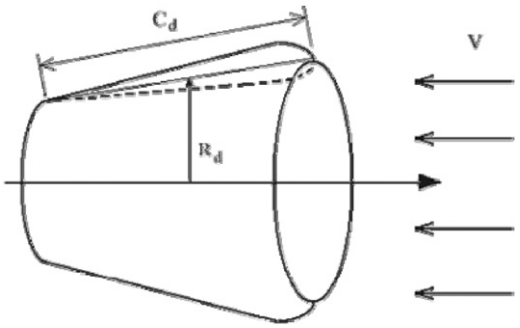

Fig. 10. Propeller duct and the flow representation.

The drag coefficient can change significantly depending on the duct profile. The experimental value for the forward thrust increase type duct is given by (Morgan and Caster, 1965)

$$(C_{D_0})_{duct} = 0.48\frac{c_d R_d}{L^2}. \quad (44)$$

The duct contribution to the total moment and rotational motion derivatives is calculated taking into account the longitudinal position of the duct leading edge, x_{LE}, and its centre x_d. The corresponding coefficients are given by

$$\Delta Z'_\alpha = -(C_{L_\alpha} + C_{D_0})_{duct}, \quad (45)$$

$$\Delta Z'_q = [(C_{L_\alpha})_{duct}x'_{LE} + (C_{D_0})_{duct}x'_d], \quad (46)$$

$$\Delta M'_\alpha = [(C_{L_\alpha})_{duct}x'_{LE} + (C_{D_0})_{duct}x'_d] + (C_{m_\alpha})_{duct}, \quad (47)$$

$$\Delta M'_q = -[(C_{L_\alpha})_{duct}(x'_{LE})^2 + (C_{D_0})_{duct}(x'_d)^2], \quad (48)$$

where

$$x'_{LE} = \frac{[x_0 - (x_{LE})_{duct}]}{L} \quad (49)$$

and

$$x'_d = \frac{[x_0 - (x_d)_{duct}]}{L}. \quad (50)$$

5. Computation of derivatives and preliminary tests

In what follows, we divide the motion of the vehicle into the vertical (diving) and horizontal (steering) planes. The corresponding derivatives are expressed as combinations of the coefficients presented in the last section, using the notation and non-dimensional approach adopted in SNAME (1950). See Tables 2 and 3. The simple addition of fin and body drag coefficients is considered, assuming no significant interaction occurs at small angles of attack and in the range of usual speeds adopted in AUV missions.

Experiments carried out by the National Institute of Oceanography (NIO) in Goa, India included a turning manoeuvre in the horizontal plane. The rudder deflection was 25° and the vehicle

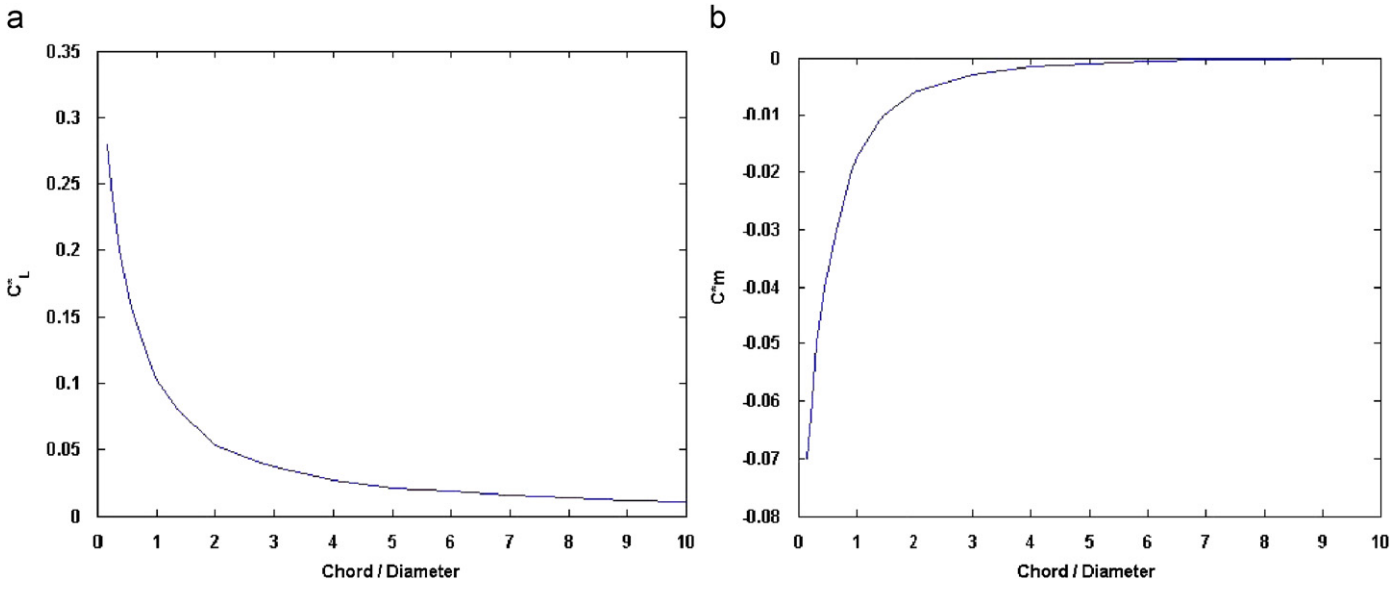

Fig. 11. (a) Duct lift coefficient slope ($C^*_L = (C_L)_{duct}/\alpha$), and (b) moment coefficient slope ($C^*_m = (C_L)_{duct}/\alpha$).

Please cite this article as: de Barros, E.A., et al., Investigation of a method for predicting AUV derivatives. Ocean Engineering (2008), doi:10.1016/j.oceaneng.2008.08.008

Table 2
Symbols and equations for longitudinal stability derivatives

Symbol	Equation
Z'_{α}	$-(C_{D_{0(B)}} + C_{D_{0(W)}} + C_{L_{\alpha(WB)}}) + \Delta Z'_{\alpha}$
Z'_{q}	$-(C_{L_{q(WB)}} + X'_{\dot{u}(B)}) + \Delta Z'_{q}$
M'_{α}	$(C_{m_{\alpha(WB)}} + \Delta M'_{\alpha}$
M'_{q}	$(C_{m_{q(WB)}} + \Delta M'_{q}$
Z'_{δ_e}	$-C_{L_{\delta_e}}$
M'_{δ_e}	$C_{m_{\delta_e}}$

Table 3
Symbols and equations for lateral stability derivatives

Symbol	Equation
Y'_{v}	$-(C_{Y_{\beta}})_{(BF)} + \Delta Z'_{\alpha}$
Y'_{r}	$(C_{Y_r})_{(BF)} + X'_{\dot{u}(B)} - \Delta Z'_{q}$
N'_{v}	$(C_{n_{\beta}})_{(BF)} - \Delta M'_{\alpha}$
N'_{r}	$(C_{n_r})_{(BF)} + \Delta M'_{q}$
Y'_{δ}	$C_{Y_{\delta_r}}$
N'_{δ}	$C_{n_{\delta_r}}$

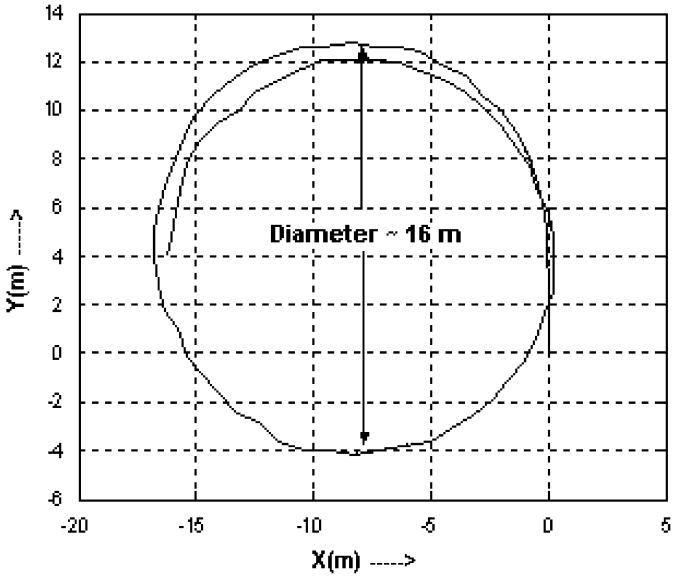

Fig. 12. Trajectory of MAYA during a turning maneuver.

speed 1.2 m/s. The resulting circular trajectory was recorded using a GPS (Fig. 12), showing a measured turning diameter of approximately 16 m, which is quite close to the 15 m value predicted according to the ASE approach. This value was calculated according to the expression for the radius R in a steady turning manoeuvre given in (Lewis, 1988)

$$\frac{R}{L} = \frac{1}{\delta}\left[\frac{Y'_{v}(N_{r'} - m'x'_{g}) - N'_{v}(Y'_{r} - m')}{N'_{v}Y'_{\delta} - Y'_{v}N'_{\delta})}\right], \tag{51}$$

where $m' = m/(\frac{1}{2}\rho L^3)$ is the non-dimensional mass of the vehicle and $x'_g = x_g/L$ is the non-dimensional longitudinal coordinate of the centre of mass.

6. Application to stern plane design

Since the hydrodynamic derivatives depend on the overall hull geometry and fin arrangement of an AUV, they are expected to play a key role in developing methodologies for vehicle design. In this paper, as an illustrative example of application of the ASE method to AUV design, we consider the problem of optimizing the manoeuvrability of an AUV in the vertical plane (when the bare hull profile is fixed) by proper choice of the stern plane dimensions and their location along the body. No ducted propeller is included, and the analysis is restricted to open-loop dynamics of the MAYA AUV, keeping its actual bare hull data (Fig. 13).

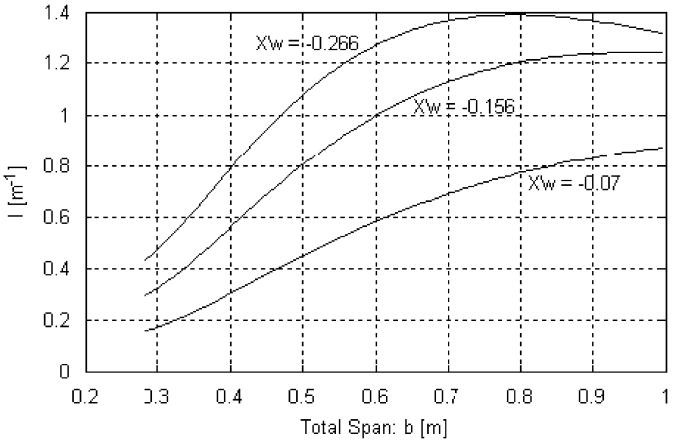

Fig. 13. Effect of the stern plane span on the manoeuvring performance.

Table 4
Coefficients of the Heave equation

a_{α}	$(m'-Z'_{\alpha})L/U$
b_{α}	Z'_{α}
c_{α}	$Z'_{q}(L/U)^2$
d_{α}	$(Z'_{q}+m')(L/U)$

The formulation of the above problem entails the definition of a performance index that will capture the manoeuvrability requirements in a rigorous manner. Suppose the objective is to achieve fast response in a surfacing/diving emergence manoeuvre (e.g. collision avoidance) while keeping the angle of attack small, well within the region of validity of a linear design model. In this case, a possible choice for the performance index is the ratio $\dot{q}(0)/\alpha_{ss}$, where α_{ss} is the steady-state value of the angle of attack in response to a stern plane step deflection and $\dot{q}(0)$ is the resulting pitch acceleration at time zero. A possible way to compute this ratio is to use the transfer functions relating the pitch angle θ and the angle of attack to the elevator deflection δ_e. These can be obtained by applying Laplace transforms to the linear equations of motion in the dive plane to yield

$$(a_{\alpha}s - b_{\alpha})\alpha(s) + (-c_{\alpha}s^2 - d_{\alpha}s)\theta(s) = Z'_{\delta_e}\delta_e(s), \tag{52}$$

$$(c_{\theta}s - d_{\theta})\alpha(s) + (a_{\theta}s^2 - b_{\theta}s - e_{\theta})\theta(s) = M'_{\delta_e}\delta_e(s). \tag{53}$$

Here, a steady forward motion at the trimming state was assumed initially, and the surge effects were neglected. The relationship between the above coefficients and the hydrodynamic derivatives is given in Tables 4 and 5, assuming that the origin O of the body-axis reference frame coincides with the centre of mass.

From the above, it is easy to obtain the transfer functions from elevator deflection δ_e to pitch and angle of attack, given by

$$\frac{\theta(s)}{\delta_e(s)} = \frac{N_{\theta}(s)}{D(s)} \tag{54}$$

Please cite this article as: de Barros, E.A., et al., Investigation of a method for predicting AUV derivatives. Ocean Engineering (2008), doi:10.1016/j.oceaneng.2008.08.008

Table 5
Coefficients of the Pitch equation

a_θ	$(I'_{yy} - M'_{\dot{q}})(L/U)^2$
b_θ	$M'_{q}(L/U)$
c_θ	$M'_{\dot{\alpha}}(L/U)$
d_θ	M'_{α}
e_θ	M'_{θ}

and

$$\frac{\alpha(s)}{\delta_e(s)} = \frac{N_\alpha(s)}{D(s)}, \tag{55}$$

respectively. Applying the initial and final value theorems to the step responses of the above transfer functions gives

$$\frac{\dot{q}(0)}{\alpha_{ss}} = \frac{M'_{\delta_e} b_\alpha}{a_\theta Z'_{\delta_e}} = -x'_w \frac{b_\alpha}{a_\theta}. \tag{56}$$

In order to simplify the analysis, suppose that the problem is limited to searching for the optimal size and location of the stern planes, considered as two rectangular non-cambered fins. Further assume that modification of the fins does not significantly change the centre of mass of the vehicle. Notice that changing the span of the fins affects both a_θ and b_α. When the span is increased, the change in b_α is mainly due to an increase in the magnitude of the lift force, whereas the change in a_θ is mainly due to an increase in the magnitude of the added moment of inertia $M'_{\dot{q}}$. To compute the change in the latter coefficient, start by computing the sectional (heave) added mass coefficient, m_{33}, of a finned circle as (Newman, 1977)

$$m_{33} = \rho\pi\left[\frac{d^2}{4} + \frac{((b_e/2)+d)^2(b_e/2)^2}{((b_e/2)+(d/2))^2}\right], \tag{57}$$

where $b_e = b - d$ is the total exposed fin span. It is then straightforward, using strip theory, to compute the contribution of the fins to the new value of $M'_{\dot{q}}$. From the expression above it is clear that the variation of $M'_{\dot{q}}$ is practically proportional to the square of the surface span. The change in b_α takes place in a more complex form, as the expressions in Section 3 indicate.

The performance index should also take into account the increase in energy consumption of the vehicle in steady motion due to the increase in fin span. Clearly, this will be due to added drag. Since the fins are rectangular and have a fixed chord, the added drag force is proportional to fin span. As a consequence, the energy penalty factor is inversely proportional to the fin span. It is also important that the performance index penalize the difficulties in vehicle handling that arise when the span assumes large values. Again, this calls for a penalty function that is inversely proportional to the span size. Based on the above considerations, the final expression adopted for the performance index is

$$I = \frac{1}{(2.3 + 2b_e)} \frac{\dot{q}'(0)}{\alpha_{ss}}. \tag{58}$$

In this study, the combined span of the fins, b, was allowed to vary between 0.3 and 1.0 m, and the stern plane location could vary in the range of 0.5 m along the middle body (i.e. the cylinder) starting from the beginning of the tail. The index in (55) was normalized in such a way as to yield the approximated value of 1 for the stern plane calculated according to the static moment balancing for the MAYA configuration. This means that the dimensions of the first fin were found by fixing its position (the furthest away from the centre of mass), and varying the chord until the combined body-fin moment coefficient $C_{m_{\alpha(WB)}}$ reached the value zero. The next fins to be tested have the same chord that was found in this case (0.168 m).

Fig. 8 shows a series of plots of the performance index versus the total span for three different locations of the stern plane. The highest curve ($x'_W = -0.266$) corresponds to the location furthest way from the vehicle centre of mass, while the lowest curve ($x'_W = -0.07$) corresponds to the closest location. The other curve ($x'_W = -0.156$) refers to an intermediate position. The stern plane at the furthest location provides the largest performance index for a span of approximately 0.8 m. Increasing the distance between the stern plane and the centre of mass allows for smaller optimal fin sizes. There is no advantage in increasing the size of the fins past the optimal value of a particular curve because the added moment of inertia takes over and the performance index curve slopes down. The performance index and the corresponding curves also suggest a method to assess the trade off between manoeuvrability and other design criteria and thus defining the stern plane location. Intermediate positions between a location that gives a poor design ($x'_W = -0.156$) and another that gives the best manoeuvrability ($x'_W = -0.266$) can provide interesting solutions without losing too much in performance (this may be the case illustrated in the intermediate curve, for example).

7. Conclusions

The use of analytical and semi-empirical estimates for the derivatives of AUVs holds great potential in the development of powerful tools for optimal vehicle design. However, care must be taken not to apply the formulas blindly but rather with sound engineering judgement. This stems from the fact that the type and particular configuration of the vehicle under study, together with the manoeuvres to be predicted, influence the parameters that must be considered and the formulae that must be chosen.

For the bare hull, the normal force coefficient predicted according to the Allen-Perkins analytical expression showed good agreement with the CFD results. Compared with the predictions given by slender body theory, the Datcom formula provided a better linear approximation to the normal force behaviour, particularly when it takes into account an intermediate value between the base and the maximum cross-sectional area. The same tendency was noted in the estimation of the lift moment coefficient. From the bounds on the estimates for these coefficients, represented graphically, one is then free to propose the most convenient form of approximation, especially for control design purposes.

As shown in the paper, the estimates obtained play a crucial role in predicting the dynamic behaviour of the vehicle long before it is built and in assessing the impact of the fin arrangement on its expected performance. This fact can be of great significance in view of the need to develop methods that can help an expert during the AUV design phase.

Future work will address comparison of the estimates that are obtained using ASE and CFD methods by taking into account the body–fin combination. Towing tank experiments will also be carried out to evaluate the precision of these estimates.

Acknowledgements

The first author is very grateful to Joao Dantas, Fabio Henrique Assis and Giovani Amianti for the CFD work, the implementation of the ASE code and the preparation of this article. This work is supported in part by the FAPESP foundation, in Brazil. The second author gratefully acknowledges the support of Adl, Portugal through the MAYASub project.

References

Allen, H.J., Perkins, E.W., 1951. A study on the effects of viscosity on flow over slender inclined bodies of revolution. NACA Report 1048.

Bohlmann, H., 1990. Berechnung hydrodynamischer koeffizienten von ubooten zur vohrhersage des bewegungsverhaltens. Ph.D. Thesis. Institut fur Shifbau der Universitat Hamburg.
Chappell, P.D., 1978. Data item 78019. ESDU-Aerodynamics.
de Barros, E.A., Pascoal, A., de Sa, E., 2004. AUV dynamics: modeling and parameter estimation using analytical, semi-empirical, and CFD methods. In: Proceedings of IFAC CAMS, Ancona, Italy.
ESDU International, Aerodynamics, 1993. Contribution of Fin to Sideforce, Yawing Moment and Rolling Moment Derivatives due to Sideslip. Data Item 82010.
Hoak, D., Finck, 1978. USAF stability and control Datcom. Wright-Paterson Air Force Base, Ohio.
Hoerner, S.F., 1985. Fluid Dynamic Lift: Practical Information Aerodynamic and Hydrodynamic Lift, 2nd ed. Author.
Humphreys, D.E., 1981. Dynamics and hydrodynamics of ocean vehicles. In: Proceedings of MTS/IEEE OCEANS, pp. 88–91.
Jorgensen, L.H., 1977. Prediction of static aerodynamic characteristics for slender bodies alone and with lifting surfaces to very high angles of attack. NASA Technical Report, TR-R-474.
Lewis, E.V., 1988. Principles of Naval Architecture, vol. II. SNAME.
Maeda, H., Tatsuta, S., 1989. Prediction method of hydrodynamic stability derivatives of an autonomous non-tethered submerged vehicle. In: Proceedings of the Eighth International Conference on Offshore Mechanics and Artic Engineering.
Morgan, W.B., Caster, E.B., 1965. Prediction of the aerodynamic characteristics of annular airfoils. DTMB Report 1830.
Myring, D.F., 1976. A theoretical study of body drag in subcritical axisymmetric flow. Aeronautical Quartely 27 (3), 186–194.
Nahon, M., 1993. Determination of undersea vehicle hydrodynamics derivatives using the USAF datcom. In: Proceedings of MTS/IEEE OCEANS'93, vol. 2, pp. 283–288.
Nahon, M., 1996. A simplified dynamics model for autonomous underwater vehicles. In: Proceedings of Symposium on Autonomous Underwater Vehicles Technology, vol. 2, pp. 373–379.
Newman, J.N., 1977. Marine Hydrodynamics, ninth ed. MIT, Cambridge, MA.
Nielsen, J.N., 1960. Missile Aerodynamics. McGraw-Hill Book Comp, Inc., New York.
Pitts, William C., Jack, N. Nielsen, George, E. Kataari, 1957. Lift and center of pressure of wing–body–tail combinations at subsonic, transonic, and supersonic speeds. Technical Report, NACA.
Prestero, T., 2001. Verification of a six-degree of freedom simulation model for the remus autonomous underwater vehicle. Master Thesis, MIT.
Ridley, P., Fontan, J., Cooke, P., 2003. Submarine dynamic modeling. In: Proceedings of Australasian Conference on Robotics and Automation. Brisbane, Australia.
Silvestre, C., Pascoal, A., Kaminer, I., Healey, A., 1998. Combined plant/controller optimization with application to autonomous underwater vehicles. In: Proceedings of CAMS'98, Fukuoka, Japan.
SNAME, The Society of Naval Architects and Marine Engineers, 1950. Nomenclature for treating the motion of a submerged body through a fuid. Technical Research Bulletin N, pp. 1–5.
Whicker, L.F., Fehlner, L.F., 1958. Free-stream characteristics of a family of low-aspect ratio, all movable control surfaces for application to ship design. Technical Report 933, David Taylor Model Basin.

Please cite this article as: de Barros, E.A., et al., Investigation of a method for predicting AUV derivatives. Ocean Engineering (2008), doi:10.1016/j.oceaneng.2008.08.008